An International Journal of Optimization and Control: Theories & Applications
ISSN: 2146-0957 eISSN: 2146-5703
Vol.15, No.4, pp.670-685 (2025)
https://doi.org/10.36922//IJOCTA025160085

RESEARCH ARTICLE

Fixed-time sliding mode control with disturbance observer and variable exponent coefficient for nonlinear systems

Zeeshan Anjum[1†], Wen-Jer Chang[2*], Muhammad Shamrooz Aslam[3†], and Rizwan Ullah[1†]

[1]School of Mechanical and Electrical Engineering, Quanzhou University of Information Engineering, Quanzhou, Fujian, China
[2]Department of Marine Engineering, National Taiwan Ocean University, Keelung, Taiwan
[3]Artificial Intelligence Research Institute, China University of Mining and Technology, Xuzhou, Jiangsu, China
zeeshananjum139@outlook.com, wjchangntou@gmail.com, shamroz_aslam@cumt.edu.cn, rizwan@qzuie.edu.cn

ARTICLE INFO

Article History:
Received: April 19, 2025
1st revised: July 9, 2025
2nd revised: July 25, 2025
Accepted: July 28, 2025
Published Online: August 20, 2025

Keywords:
Fixed-time stability
Fixed-time disturbance observer
Sliding mode variable
Variable exponent coefficient

AMS Classification:
93C85, 93C41

ABSTRACT

This article presents a novel control approach for robust fixed-time trajectory tracking in nonlinear dynamic systems affected by external disturbances and model uncertainties, utilizing a fixed-time disturbance observer. Initially, a new fast disturbance observer was designed to reliably estimate external disturbances and model uncertainties within a fixed timeframe, independent of initial conditions and without requiring strict assumptions about the nature of these disturbances and uncertainties. Based on the disturbance estimates, a new robust fixed-time trajectory tracking sliding mode control strategy was developed, incorporating a fixed-time sliding variable and a reaching law with a state-dependent exponent coefficient. Using Lyapunov-based analysis, it is proven that the tracking errors of the closed-loop system converge to a neighborhood of the origin within a fixed time, independent of the initial conditions. Finally, comprehensive simulations were conducted to validate the effectiveness of the proposed strategy, demonstrating its advantages in achieving fast convergence, avoiding singularities, reducing chattering, and compensating for model uncertainties and external disturbances.

CC BY

1. Introduction

Nonlinear dynamical systems often experience a decline in performance due to uncertainties and external disturbances. Various nonlinear control methods, such as backstepping control,[1] intelligent control,[2,3] feedback linearization control,[4,5] sliding mode control (SMC),[6,7] and optimal control,[8,9] have been developed to optimize control effectiveness in complex systems affected by model uncertainties and external disturbances.

Sliding mode control, a part of the variable structure control family, is characterized by modifications in the control law structure as system dynamics evolve over time.[10,11] It is well-known for its effectiveness in mitigating system imperfections. A recent work[12] proposed an SMC law that guarantees asymptotic convergence of trajectory tracking errors. However, while linear SMC ensures asymptotic convergence of the system state, it does not specify the convergence time. To address this limitation, the terminal SMC method was introduced in Venkataraman and Gulati,[13]

† *These authors contributed equally to this work.*
*Corresponding Author

ensuring finite-time stabilization of system states. Nonlinear terminal SMC outperforms traditional linear SMC in several ways, including lower steady-state tracking errors, convergence within a finite timeframe, and enhanced dynamic response.[14–19] However, general terminal SMC is frequently afflicted with singularity problems.[14,15] Effective solutions to this issue have been proposed, broadly categorized into direct approaches[16,17] and switching methods.[20,21] It is also worth noting that terminal SMC and linear SMC produce similar convergence rates when system states are far from equilibrium. To improve this, the concept of fast terminal SMC (FTSMC) was introduced, ensuring rapid transient convergence regardless of the distance from equilibrium.[17] Nonetheless, the convergence time in general FTSMC may become excessively long as initial system values increase. In high-performance systems, a convergence time independent of initial conditions is desirable. This need led to the emergence of fixed-time stability theory, which has inspired various fixed-time control systems.[22] The formation control challenge for multi-robot systems with time delay was addressed in Wang et al.,[23] considering both undirected and directed topologies. A cooperative control scheme combining fixed-time and switching strategies to ensure consensus in first- and second-order multi-agent systems was proposed in Du et al.[24] An adaptive fuzzy fixed-time controller was designed for robots operating under uncertainty, based on position tracking error restrictions, to ensure fast system response.[25] For the challenge of adaptive attitude control in flexible spacecraft facing unpredictable disturbances and actuator failures,[26] developed a continuous adaptive control technique that combines the sliding mode technique with a fixed-time control strategy, enhancing both the precision and stability of the spacecraft's attitude. Ahmed and Azar[15] presented a fixed-time nonsingular terminal sliding variable to robustly control second-order systems, altering the control law near the origin to avoid singularities. In Zhang et al.,[27] a terminal sliding surface tailored for fixed-time control of submarine-launched missile attitude tracking was proposed, using a sinusoidal function to address singularity issues. Ni et al.[28] developed a rapid fixed-time controller for energy storage devices using sliding mode control theory and the saturation function method to avoid singularities. Fixed-time terminal SMC techniques are also described in Wang et al.[29] and related works. Most of these rely on the fixed-time stability principles outlined in Zuo et al.[14,22,30] To achieve rapid convergence,[31] introduced a novel fixed-time stability theorem for neural network synchronization, providing a more precise settling time estimate.

Uncertainties and disturbances significantly affect control performance in nonlinear dynamical systems. Adaptive control-based disturbance rejection techniques estimate and compensate for bounds on disturbances and uncertainties, as detailed in Zhao and Jia[32] though they tend to be conservative. Based on the literature, disturbance observers (DOs) provide a robust solution by addressing both model uncertainties and external disturbances. Conventional DOs for nonlinear systems[33,34] typically assume slow-varying or constant uncertainties, which may not hold in practice. To ensure robust fixed-time stability in nonlinear systems, it is essential to observe both external disturbances and internal uncertainties within a predetermined timeframe. While finite-time DOs[35,36] offer a generic solution for correcting observation time, their observation time can become unbounded if the initial observer error is large. Furthermore, current observers often require prior knowledge of disturbance bounds or assume a zero rate of change for disturbances.[37] As a result, a fixed-time DO with less stringent constraints on both uncertainties and disturbances is required for nonlinear dynamical systems. To overcome these challenges, this study proposes a fixed-time variable exponent coefficient DO (FVECDO) that enables reliable observation of lumped disturbances, comprising both model inaccuracies and external disturbances, within a fixed time, under more relaxed assumptions.

Building on the discussion above, this paper explores a method for trajectory tracking control with fixed-time convergence in nonlinear systems affected by lumped disturbances. Specifically, an FVECDO-based fixed-time trajectory tracking sliding mode control (FTTSMC) approach is developed, incorporating a fixed-time sliding variable and a reaching strategy with a state-dependent exponent coefficient. It effectively addresses lumped disturbances, ensuring that trajectory tracking errors approach an area close to the origin within a time bound that is independent of the system's initial state. The key outcomes of this research are outlined as follows:

(i) Utilizing the error model, an FVECDO is designed to estimate lumped disturbances. Unlike finite-time Dos, this observer guarantees lumped disturbance estimation within a fixed timeframe, regardless of initial conditions. Additionally, compared to fixed-time DOs[38,39] that rely on known bounds of lumped disturbances and their derivatives, the proposed FVECDO imposes fewer constraints on these disturbances, making it more effective for practical scenarios.

(ii) To achieve stable, rapid, and precise trajectory tracking in nonlinear dynamical systems, a novel FTTSMC utilizing a reaching strategy with a state-dependent exponent coefficient is proposed. This controller, leveraging disturbance estimation information, ensures rapid convergence both near and far from the system's equilibrium point, while avoiding singularity issues.

(iii) Furthermore, fixed-time stability of the closed-loop system is analyzed using the Lyapunov method.

The structure of this paper is as follows: Section 2 introduces the foundational concepts and outlines the problem. Section 3 presents the observer-based fixed-time control method and details the fixed-time stability of the closed-loop system. In Section 4, the proposed control strategy is validated through simulations. Finally, Section 5 concludes the study.

2. Problem formulation and mathematical foundations

2.1. Problem formulation

Consider the following second-order nonlinear dynamical system with model uncertainties and external disturbances Equation (1):

$$\begin{aligned} \dot{x}_{1a} &= x_{2a} \\ \dot{x}_{2a} &= g(x) + \Delta g(x) + h(x)\tau(t) + d_a(t) \\ y_a &= x_{1a} \end{aligned} \tag{1}$$

where y_a denotes the output signal, x_{1a} and x_{2a} signify the system's state variables. The functions $g(x)$ and $h(x)$ are assumed to be smooth and nonlinear, depending on $x = [x_{1a}, x_{2a}]^T$. The term $\Delta g(x)$ represents model uncertainties, $d_a(t)$ denotes external disturbances, and $\tau(t)$ is the control input.

Let $\Xi_1 = y_a - y_{des}$ be the difference between the actual output and the desired output, and let $\Xi_2 = \dot{y}_a - \dot{y}_{des}$ be its time derivative. Here, y_{des} and $\dot{y}_{des}$ refer to the desired trajectory and its derivative with respect to time, respectively. The corresponding error dynamics for the system can be expressed as in Equation (2).

$$\begin{aligned} \dot{\Xi}_1 &= \Xi_2 \\ \dot{\Xi}_2 &= G(x) + h(x)u + D_a \end{aligned} \tag{2}$$

where $G(x) = g(x) - \ddot{y}_{des}, u = \tau(t)$ and $D_a = \Delta g(x) + d_a(t)$ represent the lumped disturbances in the second-order system.

Assumption 1: The function $h(x)$ in Equation (1) is assumed to be greater than zero. That is, there exists a real positive value b such that $h(x) > b$, $\forall x \in \Re^2$.

Assumption 2: The lumped disturbances in the second-order system are typically unknown but constrained by a positive constant η, as in Equation (3):

$$|D_a| = |\Delta g(x) + d_a(t)| \leq \eta \tag{3}$$

Assumption 3: The desired trajectory y_{des} is twice continuously differentiable with respect to time.

2.2. Mathematical foundations

Consider a general nonlinear system as given in Equation (4):

$$\dot{y} = f(y(t)), y(0) = y_0 \tag{4}$$

where $y \in \Re^n$ and $f(y(t)) : D \to \Re^n$ are nonlinear functions.

Definition 1.[40] The equilibrium point $y = 0$ of System IV is said to be finite-time stable if it satisfies Lyapunov stability, and there exists an open region $D \subseteq D_0$ containing the origin and a function $\hat{y} : D \backslash \{0\} \to (0, \infty)$ such that, for all $y_0 \in D$, the outcome $y(t, y_0)$ for $t \in (0, \hat{y}(y_0))$ satisfies $\lim_{t \to \hat{y}(y_0)} y(t, y_0) = 0$ and $y(t, y_0) = 0$ for any $t > \hat{y}(y_0)$. Specifically, when $D \in \Re^n$, the system is globally finite-time stable.

Definition 2.[41] The equilibrium point $y = 0$ of System IV is said to be fixed-time stable if it is finite-time stable and its settling time T is constrained by a value $T_{\max} > 0$, ensuring $T \leq T_{\max}$.

Definition 3.[42] The equilibrium point $y = 0$ of System IV is said to be practically fixed-time stable if it satisfies the fixed-time stability property, and there exists a specified region $\Phi \in \Re^n$ and a constant $T > 0$ such that, for all initial conditions $y_0 \in \Re^n$, the state $y(t)$ enters the region Φ within time T and remains in Φ for all $t > T$, where T does not depend on the initial conditions.

Remark 1. Unlike global fixed-time stability, practical fixed-time stability implies convergence of tracking errors to a specific region around the origin rather than to the exact origin. This concept is often more applicable to real-world scenarios, such as motors and robotic manipulator systems,[42,43] especially in controllers employing DOs or adaptive approximators.

To better understand system stability, we refer to the following key lemmas:

Lemma 1.[22,44] Let $V(y)$ be a Lyapunov function for System IV with parameters $\alpha, \beta \in \Re^+, 0 < q_1 < 1, q_2 > 1$, and $\upsilon_\iota \in \Re^+$, satisfying the inequality $\dot{V}(y) \leq -\alpha V(y)^{q_1} - \beta V(y)^{q_2} + \upsilon_\iota$. Then, the system is practically fixed-time stable, and the residual set is defined as: $R_\iota = \{y | V(y) \leq \min \left\{ (\upsilon_\iota / ((1-\upsilon_\theta)\beta))^{1/q_2}, (\upsilon_\iota / ((1-\upsilon_\theta)\alpha))^{1/q_1} \right\}\}$ where $0 < \upsilon_\theta < 1$, and the time bound for convergence is given in Equation (5):

$$T(y_0) \leq \frac{1}{\alpha(1-q_1)} + \frac{1}{\beta(q_2-1)}, \forall y_0 \in \Re^n. \quad (5)$$

Lemma 2.[45] For any constants $\varsigma > 0$ and $l \in \Re$, the following inequality holds Equation (6):

$$0 \leq |l| - |l| \tanh\left(\frac{|l|}{\varsigma}\right) \leq \varpi\varsigma \quad (6)$$

where ϖ denotes a constant that meets the condition $\varpi = e^{-\varpi-1}, e.g\ \varpi = 0.2785$.

Notation: For any real number y, the expression $\text{sig}(y)^a = |y|^a \text{sign}(y)$, with sign(.) denotes the sign function, and a is a positive constant.

3. Main results

This paper presents the design of a novel FTTSMC using FVECDO estimation for System I, aiming to ensure that the system states reach a small neighborhood of the origin within a predetermined finite time, regardless of initial conditions.

Furthermore, the controller parameters allowed for effective adjustment of the upper limit on the settling time. Figure 1 illustrates the structure of the closed-loop trajectory tracking system resulting from this control strategy.

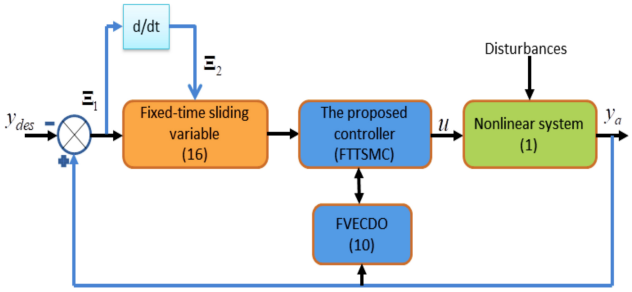

Figure 1. Block diagram of the control architecture Abbreviations: FTTSMC, fixed-time trajectory tracking sliding mode control; FVECDO, fixed-time variable exponent coefficient disturbance observer.

3.1. Fixed-time variable exponent coefficient disturbance observer design

Lumped disturbances can adversely affect the trajectory tracking performance of nonlinear dynamical systems. To improve performance, these lumped disturbances must be estimated and compensated for as early as possible. Therefore, this section introduces the FVECDO for accurate estimation of lumped disturbances, starting with a reformulation of the error model as follows:

$$\dot{\Xi}_2 = -\ell_1 \Xi_2 + h(x)u + d^* \quad (7)$$

where $d^* = G(x) + \ell_1 \Xi_2 + D_a$ and ℓ_1 denote a real positive constant. According to Equation (7), an auxiliary state $\dot{\hat{\Xi}}_2$ is introduced to define an auxiliary system as in Equation (8):

$$\dot{\hat{\Xi}}_2 = -\ell_1 \hat{\Xi}_2 + h(x)u \quad (8)$$

Let $\Theta_1 = \Xi_2 - \hat{\Xi}_2$ denote the error between the Ξ_2 and $\hat{\Xi}_2$. Substituting Equations (7) and (8) into the derivative of Θ_1 yields the following dynamics:

$$\begin{aligned} \dot{\Theta}_1 &= -\ell_1 \Theta_1 + d^* \\ \Theta_2 &= \ell_2 \Theta_1 \end{aligned} \quad (9)$$

where ℓ_2 is a real positive constant, d^* represents the unknown system input, and Θ_2 can be regarded as the system output. Using Equations (7)–(9), the FVECDO is formulated as in Equation (10):

$$\begin{aligned} \dot{\hat{\Theta}}_1 &= -\ell_2\ell_3\hat{\Theta}_1 + \ell_2^{-1}\dot{\Theta}_2 + \alpha_1\chi\left(\tilde{\Theta}_1\right)^{\phi(\tilde{\Theta}_1)}\text{sign}\left(\tilde{\Theta}_1\right) \\ &\quad + \ell_3\Theta_2 + \alpha_2\tilde{\Theta}_1 + \alpha_3\text{sig}\left(\tilde{\Theta}_1\right)^{\Upsilon} \\ \hat{d}^* &= \ell_2^{-1}\left(\ell_1\ell_2\hat{\Theta}_1 + \dot{\Theta}_2\right) \\ \hat{D}_a &= \hat{d}^* - \ell_1\Xi_2 - G(x) \end{aligned} \quad (10)$$

where $\ell_3 \in \Re^+, \alpha_1 \in \Re^+, \alpha_2 \in \Re^+$ and $\alpha_3 \in \Re^+$ are observer gains. $0 < \Upsilon < 1, \chi\left(\tilde{\Theta}_1\right)$ is employed to represent the function $\chi\left(\tilde{\Theta}_1\right) = \left|\tilde{\Theta}_1 + \text{sign}\left(\tilde{\Theta}_1\right)\right|$, where $\chi\left(\tilde{\Theta}_1\right) = 0$ if and only if $\tilde{\Theta}_1 = 0$, otherwise $\chi\left(\tilde{\Theta}_1\right) > 1$. Moreover, $\phi\left(\tilde{\Theta}_1\right)$ is expressed as $\phi\left(\tilde{\Theta}_1\right) = \left(p_1 + \lambda_1\tilde{\Theta}_1^2\right) / \left(1 + \mu_1\tilde{\Theta}_1^2\right)$, with $p_1 > 1, \lambda_1, \mu_1 > 0$, and $\lambda_1 > p_1\mu_1$. $\hat{\Theta}_1, \hat{d}^*, \hat{D}_a$ represents the estimations of Θ_1, d^*, D_a respective disturbances, and $\tilde{\Theta}_1 = \Theta_1 - \hat{\Theta}_1$ denotes the estimation error. The observer error is defined as $\tilde{D} = D_a - \hat{D}_a$, which leads to the establishment of the following theorem.

Theorem 1. The estimation error $\tilde{D}$ of the observer will reach zero within a predetermined time. In other words, there exists a positive constant $T_{Obs} \in \Re$ such that $\tilde{D} = 0$ for $t > T_{Obs}$.

Proof. The proof consists of two steps. Step 1 provides the stability analysis of $\tilde{\Theta}_1$ using Lyapunov theory, while Step 2 demonstrates the fixed-time convergence of the observer error $\tilde{D}$.

Step 1. The Lyapunov function for $\tilde{\Theta}_1$ is selected as

$$V_1 = 0.5\tilde{\Theta}_1^2 \tag{11}$$

Taking the time derivative of Equation (11) and applying Equations (9) and (10) yields:

$$\begin{aligned}
\dot{V}_1 &= \tilde{\Theta}_1\Big(\dot{\Theta}_1 + \ell_2\ell_3\hat{\Theta}_1 - \ell_2^{-1}\dot{\Theta}_2 - \ell_3\Theta_2 - \alpha_2\tilde{\Theta}_1 \\
&\quad -\alpha_1\chi\Big(\tilde{\Theta}_1\Big)^{\phi(\tilde{\Theta}_1)}\text{sign}\left(\tilde{\Theta}_1\right) - \alpha_3\text{sig}\Big(\tilde{\Theta}_1\Big)^{\Upsilon}\Big) \\
&= \tilde{\Theta}_1\Big(\dot{\Theta}_1 + \ell_2\ell_3\hat{\Theta}_1 - \ell_2^{-1}\ell_2\dot{\Theta}_1 - \ell_2\ell_3\Theta_1 - \alpha_2\tilde{\Theta}_1 \\
&\quad -\alpha_1\chi\Big(\tilde{\Theta}_1\Big)^{\phi(\tilde{\Theta}_1)}\text{sign}\left(\tilde{\Theta}_1\right) - \alpha_3\text{sig}\Big(\tilde{\Theta}_1\Big)^{\Upsilon}\Big) \\
&= \tilde{\Theta}_1\Big(-\ell_2\ell_3\tilde{\Theta}_1 - \alpha_1\chi\Big(\tilde{\Theta}_1\Big)^{\phi(\tilde{\Theta}_1)}\text{sign}\left(\tilde{\Theta}_1\right) - \alpha_2\tilde{\Theta}_1 \\
&\quad -\alpha_3\text{sig}\Big(\tilde{\Theta}_1\Big)^{\Upsilon}\Big) \\
&\le -\tilde{\Theta}_1\Big(\alpha_1\chi\Big(\tilde{\Theta}_1\Big)^{\phi(\tilde{\Theta}_1)}\text{sign}\left(\tilde{\Theta}_1\right) + \alpha_2\tilde{\Theta}_1 \\
&\quad +\alpha_3\text{sig}\Big(\tilde{\Theta}_1\Big)^{\Upsilon}\Big) \\
&\le -\alpha_1\left|\tilde{\Theta}_1\right|\left(\left|\tilde{\Theta}_1\right| + \left|\text{sign}\left(\tilde{\Theta}_1\right)\right|\right)^{\phi(\tilde{\Theta}_1)} - \alpha_2\left|\tilde{\Theta}_1\right|^2 \\
&\quad - \alpha_3\left|\tilde{\Theta}_1\right|^{\Upsilon+1} \\
&\le -\alpha_1\left|\tilde{\Theta}_1\right|\left(\left|\tilde{\Theta}_1\right| + \left|sign\left(\tilde{\Theta}_1\right)\right|\right)^{p_1} - \alpha_2\left|\tilde{\Theta}_1\right|^2 \\
&\quad - \alpha_3\left|\tilde{\Theta}_1\right|^{\Upsilon+1} \\
&\le -\alpha_1\left|\tilde{\Theta}_1\right|^{p_1+1} - \alpha_2\left|\tilde{\Theta}_1\right|^2 - \alpha_3\left|\tilde{\Theta}_1\right|^{\Upsilon+1} \\
&\le -\alpha_1 2^{\frac{p_1+1}{2}}V_1^{\frac{p_1+1}{2}} - 2\alpha_2V_1 - \alpha_3 2^{\frac{\Upsilon+1}{2}}V_1^{\frac{\Upsilon+1}{2}} \\
&= -\beta_1V_1^{\frac{p_1+1}{2}} - \beta_2V_1 - \beta_3V_1^{\frac{\Upsilon+1}{2}}
\end{aligned} \tag{12}$$

where $\beta_1 = \alpha_1 2^{\frac{p_1+1}{2}}, \beta_1 = 2\alpha_2$, and $\beta_3 = \alpha_3 2^{\frac{\Upsilon+1}{2}}$. Next, we solve Equation (12) and demonstrate that $V_1\left(\tilde{\Theta}_1\right) = 0$ can be achieved in fixed time. The following expression, denoted as Equation (13), can be obtained:

$$\begin{aligned}
T_{Obs} &\le \lim_{V_1(\tilde{\Theta}_{1_0})\to 0}\int_0^{V_1(\tilde{\Theta}_{1_0})}\frac{\mathrm{d}V_1}{\beta_1V_1^{\frac{p_1+1}{2}} + \beta_2V_1 + \beta_3V_1^{\frac{\Upsilon+1}{2}}} \\
&\le \int_0^1\frac{\mathrm{d}V_1}{\beta_2V_1 + \beta_3V_1^{\frac{\Upsilon+1}{2}}} \\
&\quad + \lim_{V_1(\tilde{\Theta}_{1_0})\to 0}\int_0^{V_1(\tilde{\Theta}_{1_0})}\frac{\mathrm{d}V_1}{\beta_1V_1^{\frac{p_1+1}{2}} + \beta_2V_1} \\
&\le \int_0^1\frac{\mathrm{d}V_1}{\beta_2V_1 + \beta_3V_1^{\frac{\Upsilon+1}{2}}} + \lim_{V_1(\tilde{\Theta}_{1_0})\to 0}\int_0^{V_1(\tilde{\Theta}_{1_0})}\frac{\mathrm{d}V_1}{\beta_1V_1^{\frac{p_1+1}{2}}} \\
&= \frac{2}{\beta_2\left(1-\Upsilon\right)}\ln\left(1 + \frac{\beta_2}{\beta_3}\right) + \frac{2}{\beta_1\left(p_1 - 1\right)}
\end{aligned} \tag{13}$$

Step 2. Referring to Equations (7) and (10), the observer error $\tilde{D}$ takes the form of

$$\begin{aligned}
\tilde{D} &= d^* - G\left(x\right) - \ell_1\Xi_2 - \hat{d}^* + \ell_1\Xi_2 + G\left(x\right) \\
&= d^* - \hat{d}^*
\end{aligned} \tag{14}$$

Subsequently, Equation (14) can be further reduced to Equation (15) by applying the estimation of d^* as specified in Equation (10):

$$\begin{aligned}
\tilde{D} &= d^* - \ell_2^{-1}\left(\ell_1\ell_2\hat{\Theta}_1 + \dot{\Theta}_2\right) \\
&= d^* - \ell_2^{-1}\left(\ell_1\ell_2\hat{\Theta}_1 - \ell_1\ell_2\Theta_1 + \ell_2d^*\right) \\
&= \ell_1\tilde{\Theta}_1
\end{aligned} \tag{15}$$

Given that $\tilde{\Theta}_1\left(t\right) = 0$ holds for $t > T_{Obs}$ as established in Step 1, it follows from Equation (15) that $\tilde{D}\left(t\right) = 0$ is also true for$t > T_{Obs}$. As a result, D_a can be reliably approximated by $\hat{D}_a$ in a fixed time, finalizing the proof.

3.2. Fixed-time trajectory tracking sliding mode control law design

In this section, employing the obtained disturbance estimation, a novel robust FTTSMC is proposed for a nonlinear dynamical system subjected

to lumped disturbances. This controller utilizes a fixed-time sliding variable and a fixed-time reaching method with a state-dependent exponent coefficient. Furthermore, it is demonstrated through Lyapunov-based analysis that the closed-loop system's tracking errors, irrespective of the initial conditions, settle in a fixed time to an area close to the origin. Consequently, a fixed-time sliding variable for the system in Equation (2) is employed as follows:

$$s = \Xi_2 + \vartheta_1 |\Xi_1|^{\Omega} \text{sign}\left(\Xi_1\right) + \vartheta_2 \tanh\left(\Xi_1/\upsilon_1\right) \tag{16}$$

where $\tanh(\cdot)$ represents the hyperbolic tangent function, and $\upsilon_1 \in (0,1)$, $\vartheta_1, \vartheta_2 > 0$, and $\Omega > 1$ denote the control parameters. Differentiating the sliding variable in Equation (16) and employing Equation (2), we arrive at Equation (17):

$$\begin{aligned} \dot{s} = {} & G\left(x\right) + h\left(x\right) u + D_a + \vartheta_1 \Omega |\Xi_1|^{\Omega-1} \Xi_2 \\ & + \left(\vartheta_2/\upsilon_1\right)\left(1 - \tanh^2\left(\Xi_1/\upsilon_1\right)\right)\Xi_2 \end{aligned} \tag{17}$$

A state-dependent exponent coefficient reaching law is designed as Equation (18):

$$\dot{s} = -\alpha_4 \chi(s)^{\phi(s)} \text{sign}\left(s\right) - \alpha_5 s - \alpha_6 \text{sign}\left(s\right) \tag{18}$$

where $\alpha_4 \in \Re^+, \alpha_5 \in \Re^+$ are controller gains, $\chi\left(s\right)$ is employed to represent the function $\chi\left(s\right) = \left|s + \text{sign}\left(s\right)\right|$, and $\chi\left(s\right) = 0$ if and only if $s = 0$, otherwise $\chi\left(s\right) > 1$. Moreover, $\phi\left(s\right)$ the time varying exponent is $\phi\left(s\right) = \left(p_2 + \lambda_2 s^2\right)/\left(1 + \mu_2 s^2\right)$, with $p_2 > 1, \lambda_2, \mu_2 > 0$ and $\lambda_2 > p_2 \mu_2$. Furthermore, α_6 is selected as shown in Equation (19):

$$\alpha_6 = \begin{cases} \alpha_6^* + \left|\hat{D}_a\right| + \eta, \ 0 \le t \le T_{Obv} \\ \alpha_6^*, \ t > T_{Obv} \end{cases} \tag{19}$$

where $\alpha_6^* \in \Re^+$. By integrating the observer estimation, the fixed-time sliding variable in Equation (19), and the reaching law in Equation (18), the FTTSMC law is formulated as given in Equation (20):

$$u = -h(x)^{-1}\left[u_a + u_b\right] \tag{20}$$

where

$$\begin{aligned} u_a = {} & G\left(x\right) + \hat{D}_a + \vartheta_1 \Omega |\Xi_1|^{\Omega-1} \Xi_2 \\ & + \left(\vartheta_2/\upsilon_1\right)\left(1 - \tanh^2\left(\Xi_1/\upsilon_1\right)\right)\Xi_2 \end{aligned} \tag{21}$$

$$u_b = \alpha_4 \chi(s)^{\phi(s)} \text{sign}\left(s\right) + \alpha_5 s + \alpha_6 \text{sign}\left(s\right) \tag{22}$$

Theorem 2. Applying the FTTSMC law in Equation (20) to the nonlinear system in Equation (2) facilitates the convergence of trajectory tracking errors to a minimal residual set, with settling time satisfying Equations (23) and (24):

$$T_r{}' \le \frac{2}{\beta_5} \ln\left(1 + \frac{\beta_5}{\beta_6}\right) + \frac{2}{\beta_4\left(p_2 - 1\right)} \tag{23}$$

$$T' \le T_r{}' + \frac{2}{\chi_1\left(\Omega + 1\right)} + \frac{2}{\chi_2} \tag{24}$$

Proof. The controller constructed using sliding mode control theory has the characteristic that the control process can be divided into two stages. Accordingly, the proof will be carried out in two stages.

Stage 1. By selecting a Lyapunov candidate $V_2 = 0.5 s^2$ and using Equation (17), the time derivative of this Lyapunov candidate yields the expression in Equation (25):

$$\begin{aligned} \dot{V}_2 = {} & s\Big(G\left(x\right) + h\left(x\right) u + \hat{D}_a + \vartheta_1 \Omega |\Xi_1|^{\Omega-1} \Xi_2 \\ & + \left(\vartheta_2/\upsilon_1\right)\left(1 - \tanh^2\left(\Xi_1/\upsilon_1\right)\right)\Xi_2\Big) \end{aligned} \tag{25}$$

If Assumption 2 holds, Equation (26) can be obtained

$$\begin{aligned} \dot{V}_2 &= s\left(-\alpha_4 \chi(s)^{\phi(s)} \text{sign}\left(s\right) - \alpha_5 s - \alpha_6 \text{sign}\left(s\right) + \tilde{D}\right) \\ &\le -\alpha_4 |s| \left(|s| + |\text{sign}\left(s\right)|\right)^{\phi(s)} - \alpha_5 |s_1|^2 - \left(\alpha_6 - \left|\tilde{D}\right|\right)|s| \\ &\le -\alpha_4 |s| \left(|s| + |\text{sign}\left(s\right)|\right)^{p_2} - \alpha_5 |s|^2 - \left(\alpha_6 - \left|\tilde{D}\right|\right)|s| \\ &\le -\alpha_4 |s|^{p_2+1} - \alpha_5 |s|^2 - \left(\alpha_6 - \left|\tilde{D}\right|\right)|s| \end{aligned} \tag{26}$$

by using Equation (19). For $0 \le t \le T_{Obs}$, the estimation error of the lumped disturbances satisfies $\left|\hat{D}_a\right| + \eta \ge \left|\tilde{D}\right|$, which implies $\alpha_6 - \left|\tilde{D}\right| \ge \alpha_6^*$. Furthermore, Theorem 1 states that the estimation error of the lumped disturbances is zero for $t \ge T_{Obs}$, implying that $\alpha_6 - \left|\tilde{D}\right| = \alpha_6^*$. According to this approach, Equation (26) can be recast as follows:

$$\begin{aligned} \dot{V}_2 &\le -\alpha_4 2^{\frac{p_2+1}{2}} V_2^{\frac{p_2+1}{2}} - 2\alpha_5 V_2 - \alpha_6^* \sqrt{2} V_2^{\frac{1}{2}} \\ &= -\beta_4 V_2^{\frac{p_2+1}{2}} - \beta_5 V_2 - \beta_6 V_2^{\frac{1}{2}} \end{aligned} \tag{27}$$

where $\beta_4 = \alpha_4 2^{\frac{p_2+1}{2}}$, $\beta_2 = 2\alpha_5$, and $\beta_6 = \alpha_6^* \sqrt{2}$. Based on earlier analysis, Equation (27) replicates the structure of Equation (11). As a result, will be attained, regardless of its initial value, within a specific timeframe $T_r{}' \le \frac{2}{\beta_5} \ln\left(1 + \frac{\beta_5}{\beta_6}\right) + \frac{2}{\beta_4(p_2-1)}$.

Stage 2. The convergence of the tracking error is demonstrated in this stage. As previously

stated, the state-dependent exponent coefficient reaching law in Equation (18) ensures that $s = 0$ is attained within a specific timeframe. Therefore, from Equation (16) it follows that:

$$\Xi_2 = -\left(\vartheta_1|\Xi_1|^{\Omega}\text{sign}\left(\Xi_1\right) + \vartheta_2 \tanh\left(\Xi_1/\upsilon_1\right)\right) \tag{28}$$

Consider the Lyapunov function defined as $V_3 = 0.5\Xi_1^2$. By differentiating it with respect to time, we get:

$$\begin{aligned} V_3 &= \Xi_1\left(-\vartheta_1|\Xi_1|^{\Omega}\text{sign}\left(\Xi_1\right) - \vartheta_2 \tanh\left(\Xi_1/\upsilon_1\right)\right) \\ &= -\vartheta_1|\Xi_1|^{\Omega+1} - \vartheta_2\Xi_1 \tanh\left(\Xi_1/\upsilon_1\right) \\ &\leq -\vartheta_1|\Xi_1|^{\Omega+1} - \vartheta_2\left|\Xi_1\right| + \vartheta_2\varpi\upsilon_1 \\ &\leq -\chi_1 V_3^{\frac{\Omega+1}{2}} - \chi_2 V_3^{\frac{1}{2}} + \vartheta_2\varpi\upsilon_1 \end{aligned} \tag{29}$$

where $\chi_1 = \vartheta_1 2^{\frac{\Omega+1}{2}}$ and $\chi_2 = \sqrt{2}\vartheta_2$. According to Lemma 1, the trajectory tracking error Ξ_1 approaches an area near zero within a fixed-time duration $T_s{}' \leq \frac{2}{\chi_1(\Omega+1)} + \frac{2}{\chi_2}$. Moreover, the closed-loop system will reach a vicinity of zero within a fixed time $T' \leq T_r{}' + T_s{}'$.

Remark 2: The fixed-time sliding mode variable in Equation (16) employs a hyperbolic tangent function rather than a signum function to mitigate chattering. A smaller increases the approximation accuracy to the sign function. However, setting this parameter too low can cause spikes in the control output, adversely affecting system performance. Additionally, as shown in Equation (29), the parameter $\vartheta_2\varpi\upsilon_1$ negatively impacts error convergence performance. Therefore, the gain ϑ_2 should be chosen as a small constant to optimize the trade-off between reducing chattering and ensuring timely convergence.

To reduce chattering in the control generated by $\alpha_6\text{sign}\left(s\right)$, the sign function can be substituted with a hyperbolic tangent function. Additionally, to mitigate the chattering resulting from $\alpha_4\chi(s)^{\phi(s)}$, a variable gain represented as $\psi\left(s\right)$ is designed. Consequently, the control law in Equation (22) is modified as follows:

$$u_b = \psi\left(s\right)\chi(s)^{\phi(s)}\text{sign}\left(s\right) + \alpha_5 s + \alpha_6 \tanh\left(s/\upsilon_1\right) \tag{30}$$

where $\psi\left(s\right) = \left[1 + c_1 - 1/\left(1 + c_2|s|^{c_3}\right)\right]c_4.\, c_2, c_3 > 0, c_4 > 1$, and $c_1 < 1/c_4$ represent real values. The stability analysis is unaffected by $\psi\left(s\right)$, as it is positive. When the sliding mode variable in Equation (16) is far from zero, $\psi\left(s\right)$approaches $\left(1 + c_1\right)c_4 > 1$, which improves the convergence rate. Conversely, as the sliding mode variable approaches zero, $\psi\left(s\right)$ approaches $\iota = c_1c_4 < 1$, resulting in reduced chattering. However, this may slow the convergence rate. This issue is addressed by inserting the linear term $\alpha_5 s$. Therefore, the proposed scheme ensures rapid convergence during the transient state and reduces chattering in the steady state.

By substituting Equation (22) with Equation (30), the inequality in Equation (26) from the proof of Theorem 2 can be rewritten as shown in Equation (31):

$$\begin{aligned} \dot{V}_2 &= s\left(-\psi\left(s\right)\chi(s)^{\phi(s)}\text{sign}\left(s\right) - \alpha_5 s - \alpha_6 \tanh\left(s/\upsilon_1\right) + \tilde{D}\right) \\ &\leq -\iota\chi(s)^{\phi(s)}\left|s\right| - \alpha_5|s_1|^2 - \left(\alpha_6 - \left|\tilde{D}\right|\right)|s| + \alpha_6\varpi\upsilon_1 \end{aligned} \tag{31}$$

Given that $\phi\left(s\right) = \left(p_2 + \lambda_2 s^2\right)/\left(1 + \mu_2 s^2\right) \geq p_2$ is true when $p_2 > 1, \lambda_2, \mu_2 > 0$ and $\lambda_2 > p_2\mu_2$, it follows that:

$$\begin{aligned} -\iota\chi(s)^{\phi(s)}\left|s\right| &= -\iota|s + \text{sign}\left(s\right)|^{\left(p_2+\lambda_2 s^2\right)/\left(1+\mu_2 s^2\right)}\ |s| \\ &\leq -\iota(|s| + |\text{sign}\left(s\right)|)^{p_2}\left|s\right| \\ &\leq -\iota|s|^{p_2+1} \end{aligned} \tag{32}$$

By substituting Equation (32) into Equation (31) and based on the previous analysis, we obtain:

$$\begin{aligned} \dot{V}_2 &\leq -\iota|s|^{p_2+1} - \alpha_5|s_1|^2 - \left(\alpha_6 - \left|\tilde{D}\right|\right)|s| + \alpha_6\varpi\upsilon_1 \\ &\leq -\chi_3 V_2^{\frac{p_2+1}{2}} - \chi_4 V_2 - \chi_5 V_2^{\frac{1}{2}} + \alpha_6\varpi\upsilon_1 \end{aligned} \tag{33}$$

where $\chi_3 = \iota 2^{\frac{p_2+1}{2}}, \chi_4 = 2\alpha_5$ and $\chi_5 = \alpha_6^*\sqrt{2}$. Equation (33) can take three forms:

$$\begin{aligned} \dot{V}_2 \leq &-\left(1 - \delta_0\right)\chi_3 V_2^{\frac{p_2+1}{2}} - \delta_0\chi_3 V_2^{\frac{p_2+1}{2}} \\ &- \chi_4 V_2 - \chi_5 V_2^{\frac{1}{2}} + \alpha_6\varpi\upsilon_1 \end{aligned} \tag{34}$$

$$\begin{aligned} \dot{V}_2 \leq &-\chi_3 V_2^{\frac{p_2+1}{2}} - \chi_4 V_2 - \left(1 - \delta_0\right)\chi_5 V_2^{\frac{1}{2}} \\ &- \delta_0\chi_5 V_2^{\frac{1}{2}} + \alpha_6\varpi\upsilon_1 \end{aligned} \tag{35}$$

$$\begin{aligned} \dot{V}_2 \leq &-\chi_3 V_2^{\frac{p_2+1}{2}} - \left(1 - \delta_0\right)\chi_4 V_2 - \delta_0\chi_4 V_2 \\ &- \chi_5 V_2^{\frac{1}{2}} + \alpha_6\varpi\upsilon_1 \end{aligned} \tag{36}$$

where $\delta_0 \in (0, 1)$. In the case of inequality in Equation (34), if $-\left(1 - \delta_0\right)\chi_3 V_2^{\frac{p_2+1}{2}} + \alpha_6\varpi\upsilon_1 \leq 0$ is true, it can be rewritten as:

$$\dot{V}_2 \leq -\delta_0\chi_3 V_2^{\frac{p_2+1}{2}} - \chi_4 V_2 - \chi_5 V_2^{\frac{1}{2}} \tag{37}$$

It can be observed that the form of Equation (37) is the same as that of Equation (12), and the convergence area of the sliding variable is determined as shown in Equation (38):

$$\lim_{t\to T'_{r1}} |s| \leq \sqrt{2\left(\frac{\alpha_6 \varpi \upsilon_1}{\chi_3 (1-\delta_0)}\right)^{\frac{2}{p_2+1}}} \tag{38}$$

where T'_{r1} can be expressed as:

$$T'_{r1} \leq \frac{2}{\chi_4} \ln\left(1+\frac{\chi_4}{\chi_5}\right) + \frac{2}{\delta_0 \chi_3 (p_2-1)} \tag{39}$$

By applying an analogous evaluation to Equations (35) and (36), the ultimate fixed-time sliding variable is expected to reach the region defined below.

$$\Phi = \left\{ \lim_{t\to T'_r} \left| |s| \leq \min\left\{ \sqrt{2\left(\frac{\alpha_6 \varpi \upsilon_1}{\chi_3 (1-\delta_0)}\right)^{\frac{2}{p_2+1}}}, \sqrt{2\left(\frac{\alpha_6 \varpi \upsilon_1}{\chi_4 (1-\delta_0)}\right)}, \sqrt{2\left(\frac{\alpha_6 \varpi \upsilon_1}{\chi_5 (1-\delta_0)}\right)^2} \right\} \right\} \tag{40}$$

The upper bound for the fixed convergence time is represented as:

$$T'_r \leq \max\left[\begin{array}{l} \frac{2}{\chi_4} \ln\left(1+\frac{\chi_4}{\chi_5}\right) + \frac{2}{\delta_0 \chi_3 (p_2-1)}, \\ \frac{2}{\delta_0 \chi_4} \ln\left(1+\frac{\delta_0 \chi_4}{\chi_5}\right) + \frac{2}{\chi_3 (p_2-1)}, \\ \frac{2}{\chi_4} \ln\left(1+\frac{\chi_4}{\delta_0 \chi_5}\right) + \frac{2}{\chi_3 (p_2-1)} \end{array} \right] \tag{41}$$

4. Simulation and discussion

In this section, the developed control technique, FTTSMC, is implemented on two systems: a single inverted pendulum (SIP) system and a robotic manipulator system. Example 1 focuses on the SIP, a benchmark nonlinear system, to verify fixed-time convergence and robustness under relatively simple dynamics. Example 2, on the other hand, involves a more complex robotic manipulator, highlighting the scalability of the proposed controller in handling high-dimensional nonlinear systems. Simulations are conducted using MATLAB/Simulink software, employing the Runge–Kutta solver with a time step of 1 millisecond (ms), to illustrate the efficacy and superiority of the proposed control approach.

4.1. Example 1

Consider the SIP from Zuo[14] as an example. Its dynamics can be expressed in the same form as Equation (1), with $g(x)$, $h(x)$, and D_a defined as follows:

$$\begin{aligned} g(x) &= \frac{9.8\sin(x_{1a}) - 0.05\sin(x_{1a})\cos(x_{1a})(x_{2a})^2/1.1}{0.5\times[4/3 - 0.1\cos^2(x_{1a})/1.1\ ]} \\ h(x) &= \frac{\cos(x_{1a})/1.1}{0.5\times[4/3 - 0.1\cos^2(x_{1a})/1.1\ ]} \\ D_a &= \sin(10x_{1a}) + \cos(x_{2a}) \end{aligned} \tag{42}$$

where x_{1a} denotes the SIP's angular position, x_{2a} its angular velocity, and u represents the input force. During the simulations, the initial conditions are configured as $x_{1a}(0) = 1\,\text{rad}$ and $x_{2a}(0) = 0.5\,\text{rad/s}$, with the desired angular position set to $y_{\text{des}} = \sin(\pi t/2\ )\,\text{rad}$. The proposed controller, FTTSMC, is compared with Li and Cai's[46] fixed-time controller, Yang and Yang's[47] finite-time controller, and Moulay's variable exponent coefficient fixed-time controller from Moulay et al.[48] to highlight the benefits of the proposed technique. The parameters of our FVECDO-based controller are selected as: $\ell_1 = 0.03, \ell_2 = 12, \ell_3 = 21, \alpha_1 = 1, \alpha_2 = 1, \alpha_3 = 1, \alpha_5 = 1, p_1 = 1.3, \lambda_1 = 0.4, \mu_1 = 0.1, \Upsilon = 0.6, \vartheta_1 = 1.5, \vartheta_2 = 0.3, \Omega = 1.2, \upsilon_1 = 0.001, p_2 = 1.25, \lambda_2 = 0.25, \mu_2 = 0.1, c_1 = 0.4, c_2 = 5, c_3 = 0.5, c_4 = 1.5, \alpha_6^* = 0.6$. Below are the sliding variable and the control formulation presented by Li and Cai[46]:

$$s = \text{sig}(\Xi_1)^{b_1} + \frac{\bar{a}_2 b_2}{2b_2-1}\text{sig}\Big(\Xi_2 + \bar{a}_1 \text{sig}(\Xi_1)^{b_1}\Big)^{2-1/b_2} \tag{43}$$

$$\begin{aligned} u = -h(x)^{-1}\Bigg[& G(x) + \bar{a}_1 b_1 |\Xi_1|^{b_1-1}\left(\frac{\bar{\phi}}{\bar{a}_1} + \Xi_2\right) \\ & + c_1 \text{sig}(s)^{o_1} + c_2 \text{sig}(s)^{o_2} + k'\frac{e^{\bar{\rho}s}-1}{e^{\bar{\rho}s}+1}\Bigg] \end{aligned} \tag{44}$$

$$\begin{aligned} \bar{\phi} = & \frac{1}{\bar{a}_2}\text{sig}\Big(\Xi_2 + \bar{a}_1 \text{sig}(\Xi_1)^{b_1}\Big)^{1/b_2} \\ & + \frac{\bar{a}_1 b_2}{2b_2-1}\Big(\Xi_2 + \bar{a}_1 \text{sig}(\Xi_1)^{b_1}\Big) \end{aligned} \tag{45}$$

The parameters in the above expressions are selected as: $\bar{a}_1 = 3, \bar{a}_2 = 0.1, b_1 = 1.1, b_2 = 1.1, c_1 = c_2 = 1, o_1 = 5/3\, o_2 = 5/9\ , k' = 2, \bar{\rho} = 100$. Furthermore, the control law developed by Yang and Yang,[47] along with the sliding variable s, is stated as:

$$s = \Xi_1 + \bar{a}_1 \text{sig}(\Xi_1)^{b_1} + \bar{a}_2 \text{sig}(\Xi_2)^{b_2} \tag{46}$$

$$u = -h(x)^{-1}\left[G(x) - \frac{1}{\bar{a}_2 b_2}\mathrm{sig}\left(\Xi_2\left(1+\bar{a}_1 b_1|\Xi_1|^{b_1-1}\right)\right)^{2-b_2} + c_1\mathrm{sig}(s)^{o_1} + c_2\mathrm{sig}(s)^{o_2} + k'\frac{e^{\bar{\rho}s}-1}{e^{\bar{\rho}s}+1}\right] \tag{47}$$

The parameters in the above expressions are selected as follows: $\bar{a}_1 = 5, \bar{a}_2 = 0.1, b_1 = 1.1, b_2 = 1.1, c_1 = c_2 = 1, o_1 = 5/3$,$o_2 = 5/9, k' = 2, \bar{\rho} = 100$. The parameters for Moulay's variable exponent coefficient fixed-time controller are set as in Moulay et al.[48] The angular position tracking of the SIP and the angular position tracking error are illustrated in Figures 2 and 3, respectively. Additionally, the angular velocity tracking of the SIP and the angular velocity tracking error are depicted in Figures 4 and 5, respectively. The figures demonstrate that among the four controllers, the proposed FTTSMC exhibits superior performance, with faster convergence and better steady-state control accuracy in the presence of lumped disturbances. Furthermore, Figure 6 displays the lumped disturbances and their estimation, highlighting that the FVECDO performs exceptionally well by accurately estimating the lumped disturbances within a fixed-timeframe.

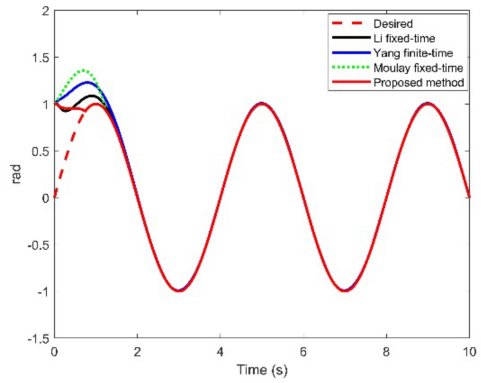

Figure 2. Angular position tracking results

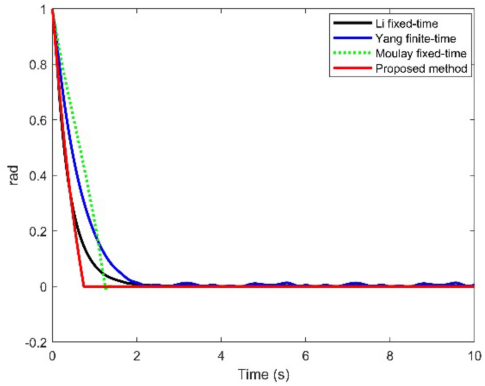

Figure 3. Position tracking errors over time

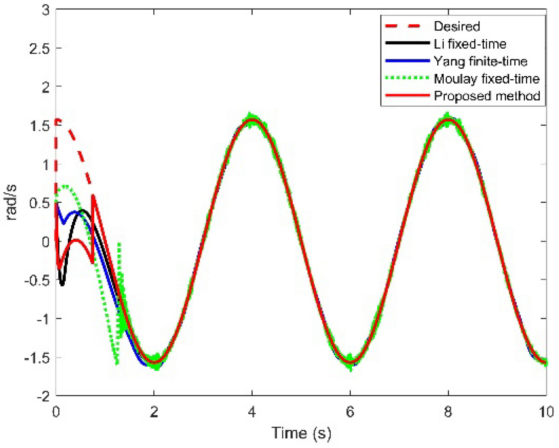

Figure 4. Angular velocity tracking results

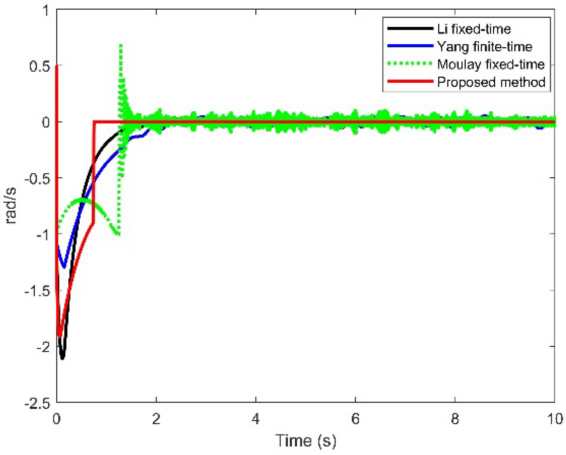

Figure 5. Angular velocity tracking error over time

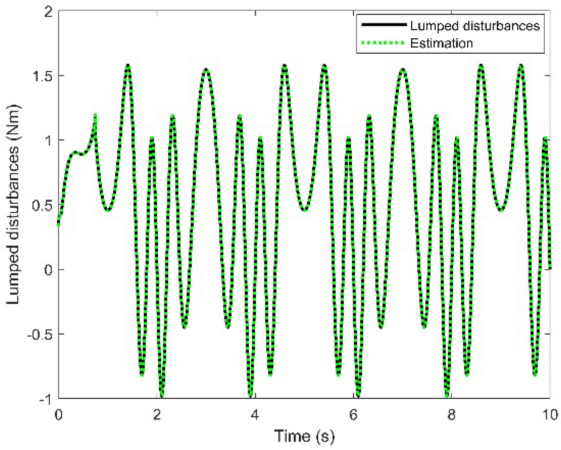

Figure 6. Estimated lumped disturbances

Three distinct sets of initial state conditions IV1 $= [x_{1a}, x_{2a}] = [1\,\mathrm{rad}, 0.5\,\mathrm{rad/s}]$, IV2 $= [x_{1a}, x_{2a}] = [3\,\mathrm{rad}, 0.0\,\mathrm{rad/s}]$,IV3 $= [x_{1a}, x_{2a}] = [5\,\mathrm{rad}, 1\,\mathrm{rad/s}]$ are used in the second phase of the SIP simulations to assess the effectiveness of the

proposed control approach under external disturbances and model uncertainties. The parameters of the FTTSMC scheme are tuned based on the earlier analysis. Tracking errors for angular position are shown in Figure 7, and tracking errors for angular velocity under various initial conditions are shown in Figure 8. It is noteworthy that the convergence time remains unchanged regardless of the initial conditions, which reinforces the fixed-time attributes discussed in this study and illustrates the practical utility of the fixed-time controller.

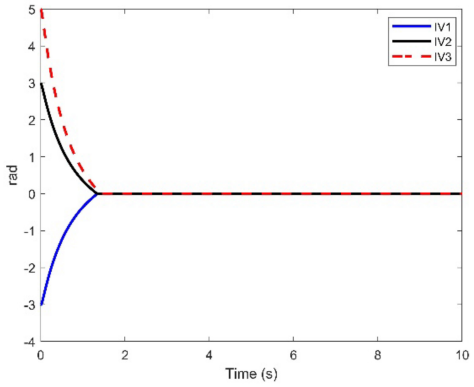

Figure 7. Position tracking errors under different initial conditions
Abbreviation: IV: initial values.

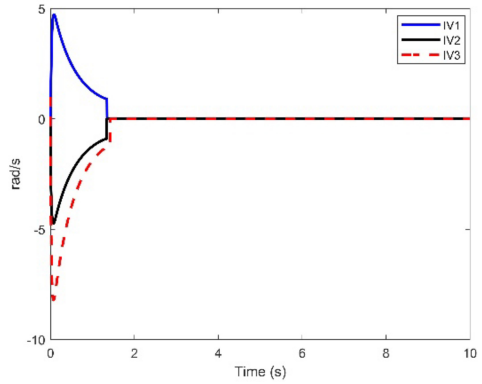

Figure 8. Velocity tracking errors under different initial conditions
Abbreviation: IV: initial values.

4.2. Example 2

The dynamic model of a standard two-link robotic manipulator, as presented in Zhai and Xu,[49] is described by the following Euler–Lagrange formulation:

$$M(q_\iota)\,\ddot{q}_\iota + Z_\iota(q_\iota,\dot{q}_\iota)\,\dot{q}_\iota + G_\iota(q_\iota) = \tau + \tau_d \quad (48)$$

where the symbol $\mathrm{M}(\mathrm{q}_\iota) \in \Re^{n\times n}$ represents the inertia matrix, which is always positive definite. $\mathrm{q}_\iota \in \Re^n$ denotes the position vector, while $\dot{q}_\iota \in \mathbb{R}^n$ and $\ddot{q}_\iota \in \mathbb{R}^n$ represent the velocity and acceleration vectors, respectively. $\tau \in \Re^n$ stands for the actuator inputs applied to the system. The matrix $Z_\iota(q_\iota,\dot{q}_\iota) \in \mathbb{R}^{n\times n}$ accounts for centripetal and Coriolis forces. $\mathrm{G}_\iota(\mathrm{q}_\iota) \in \Re^n$ represents the gravity vector, and $\tau_d \in \Re^n$ indicates the external disturbance matrix. Assume that the model parameters are expressed as $M(q_\iota) = M_0(q_\iota) + \Delta M(q_\iota), Z_\iota(q_\iota,\dot{q}_\iota) = Z_{\iota 0}(q_\iota,\dot{q}_\iota) + \Delta Z_\iota(q_\iota,\dot{q}_\iota)$, and $M(q_\iota) = M_0(q_\iota) + \Delta M(q_\iota), Z_\iota(q_\iota,\dot{q}_\iota) = Z_{\iota 0}(q_\iota,\dot{q}_\iota) + \Delta Z_\iota(q_\iota,\dot{q}_\iota), G_\iota(q_\iota) = G_{\iota 0}(q_\iota) + \Delta G_\iota(q_\iota)$, represent the nominal values. $\Delta M(q_\iota)$, $\Delta Z_\iota(q_\iota,\dot{q}_\iota)$, $\Delta G_\iota(q_\iota)$ and $\Delta M(q_\iota)$, $\Delta Z_\iota(q_\iota,\dot{q}_\iota)$, $\Delta G_\iota(q_\iota)$ represent the unknown components. The involved matrices are defined as shown in Equation (49):

$$\mathrm{M}(\mathrm{q}_\iota) = \begin{bmatrix} m_{11} & m_{12} \\ m_{21} & m_{22} \end{bmatrix}, \mathrm{Z}_\iota(\mathrm{q}_\iota,\dot{\mathrm{q}}_\iota) = \begin{bmatrix} z_{11} & z_{12} \\ z_{21} & z_{22} \end{bmatrix}, \quad \mathrm{G}(\mathrm{q}_\iota) = \begin{bmatrix} g_1 & g_2 \end{bmatrix}^T \quad (49)$$

where $\mathrm{q}_\iota = [q_{\iota 1}, q_{\iota 2}]^T$ represents the joint angle position vector of joints, $m_{11} = (m_1+m_2)\,l_1^2 + m_2 l_2^2 + 2m_2 l_1 l_2 \cos(q_{\iota 2}) + \bar{J}_1, m_{12} = m_{21} = m_2 l_2^2 + m_2 l_1 l_2 \cos(q_{\iota 2}), m_{22} = m_2 l_2^2 + \bar{J}_2, z_{11} = -m_2 l_1 l_2 \sin(q_{\iota 2})\,\dot{q}_{\iota 2}, z_{12} = -m_2 l_1 l_2 \sin(q_{\iota 2})\,(\dot{q}_{\iota 1}+\dot{q}_{\iota 2}), z_{21} = m_2 l_1 l_2 \sin(q_{\iota 2})\,\dot{q}_{\iota 1}, z_{22} = 0, g_1 = (m_1+m_2)\,9.8 l_1 \cos(q_{\iota 1}) + m_2 9.8 l_2 \cos(q_{\iota 1}+q_{\iota 2}), g_2 = m_2 9.8 l_2 \cos(q_{\iota 1}+q_{\iota 2})$. l_1, l_2, m_1 and m_2 are the length and mass of the joints, $\bar{J}_1$ and $\bar{J}_2$ indicate the inertia of the two links. The rigid two-link robotic manipulator is depicted in Figure 9. The parameter values are $m_1 = 0.5\mathrm{kg}, m_2 = 1.5\mathrm{kg}, l_1 = 1\mathrm{m}, l_2 = 0.8\mathrm{m}, \bar{J}_1 = 5\mathrm{kg\,m}^2$ and $\bar{J}_2 = 5\mathrm{kg\,m}^2$.

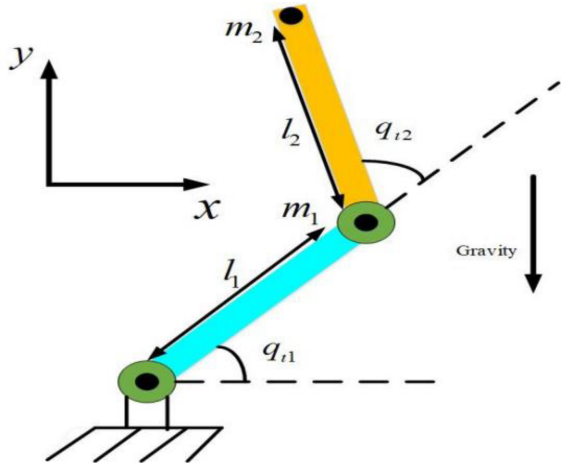

Figure 9. Architecture of a two-link robotic manipulator

By defining $x = [x_{1a}, x_{2a}]^T = [q_\iota, \dot{q}_\iota]^T$, Equation (48) can be reformulated in a manner consistent with Equation (2), with matrices $g(x)$, $h(x)$, and D_a defined as follows: $g(x) = \mathrm{M}_0^{-1}(x_{1a})(-\mathrm{Z}_{\iota 0}(x)x_{2a} - \mathrm{G}_{\iota 0}(x_{1a})), h(x) = \mathrm{M}_0^{-1}(x_{1a})D_a = \mathrm{M}_0^{-1}(x_{1a})\,(\mathrm{l}_d - \Delta \mathrm{M}(x_{1a})\,\dot{x}_{2a}$

$-\Delta \mathrm{Z}_\iota(x)x_{2a} - \Delta \mathrm{G}_\iota(x_{1a})$ The disturbance term in the model is expressed as given in Equation (50):

$$\tau_d = \begin{bmatrix} 6\sin(2t) + 2\cos(\pi t)\,(\mathrm{Nm}) \\ 5\cos(2t) + \sin(\pi t)\,(\mathrm{Nm}) \end{bmatrix} \tag{50}$$

The desired trajectories for the system are defined as shown in Equation (51):

$$y_{des} = \begin{bmatrix} 0.2\cos(0.7t) + 0.2\cos(0.5t - 0.2)\,(\mathrm{rad}) \\ 0.2\cos(0.5t - 0.2) - 0.2\cos(0.7t)\,(\mathrm{rad}) \end{bmatrix} \tag{51}$$

To illustrate the improved effectiveness of the proposed FTTSMC controller in the presence of lumped disturbances, a comparative assessment is carried out against Boukattaya et al.'s[50] controller. Based on Theorem 2, the proposed FTTSMC controller for the ith degree of freedom in the system described by Equation (48) is formulated as given in Equation (52):

$$u_i = -h\,(x)_i^{-1}\,[u_{ai} + u_{bi}] \tag{52}$$

where

$$\begin{aligned} u_{ai} = {} & G(x)_i + \hat{D}_{ai} + \vartheta_1 \Omega |\Xi_{1i}|^{\Omega - 1}\Xi_{2i} \\ & + (\vartheta_2/\upsilon_1\,)\left(1 - \tanh^2\left(\Xi_{1i}/\upsilon_1\,\right)\right)\Xi_{2i} \end{aligned} \tag{53}$$

$$u_{bi} = \psi\,(s_i)\,\chi(s_i)^{\phi(s_i)}\mathrm{sign}\,(s_i) + \alpha_5 s_i + \alpha_6 \tanh\,(s_i/\upsilon_1\,) \tag{54}$$

The parameters of our FVECDO-based controller are selected as:$\ell_1 = 0.03, \ell_2 = 12, \ell_3 = 21, \alpha_1 = 1, \alpha_2 = 1\ , \alpha_3 = 1, \alpha_5 = 1, p_1 = 1.3, \lambda_1 = 0.4, \mu_1 = 0.1, \Upsilon = 0.6, \vartheta_1 = 1.5, \vartheta_2 = 0.3, \Omega = , \upsilon_1 = 0.001, p_2 = 1.25, \lambda_2 = 0.25, \mu_2 = 0.1, c_1 = 0.4, c_2 = 5, c_3 = 0.5, c_4 = 1.5, \alpha_6^* = 0.6.$

As outlined in Ref.,[50] Boukattaya et al.'s controller is structured as follows:

$$s = q'_1 + b'_1 \left|q'_1\right|^{\alpha'} \mathrm{sign}\left(q'_1\right) + b'_2 \left|q'_2\right|^{\beta'} \mathrm{sign}\left(q'_2\right) \tag{55}$$

$$\begin{aligned} u = {} & \mathrm{Z}_{\iota 0}(\mathrm{q}_\iota, \dot{}_\iota)_\iota + \mathrm{G}_{\iota 0}(\mathrm{q}_\iota) + \mathrm{M}_0(\mathrm{q}_\iota)\ddot{y}'_d \\ & - \frac{\mathrm{M}_0(\mathrm{q}_\iota)}{b'_2\beta'}\left|q'_2\right|^{2-\beta}\left(1 + b'_1\alpha'\left|q'_1\right|^{\alpha-1}\right)\mathrm{sign}\left(q'_2\right) \\ & - \mathrm{M}_0(\mathrm{q}_\iota)\left(k'.s + \left(\hat{b}_0 + \hat{b}_1\left|q_\iota\right| + \hat{b}_2|\dot{q}_\iota|^2 + \xi\right)\mathrm{sign}(s)\right) \end{aligned} \tag{56}$$

$$\begin{aligned} \dot{\hat{b}}_0 &= \lambda_0\,|s|\,\left|q'_2\right|^{\beta'-1} \\ \dot{\hat{b}}_1 &= \lambda_1\,|s|\,|q_\iota|\,\left|q'_2\right|^{\beta'-1} \\ \dot{\hat{b}}_2 &= \lambda_2\,|s|\,|\dot{q}_\iota|^2\left|q'_2\right|^{\beta'-1} \end{aligned} \tag{57}$$

The parameters of the Boukattaya et al.'s[50] controller outlined above are stated as:$\alpha' = 2, \beta' = 5/3\ , \xi = 2, b'_1 = b'_2 = 1, k = 2, \lambda_0 = \lambda_1 = \lambda_2 = 1.$ The initial conditions for the joint positions are selected as $q_{\iota 1}\,(0) = 1\mathrm{rad}$, and $q_{\iota 2}\,(0) = 0.2\,\mathrm{rad}$. Figures 10 and 11 show the position tracking performance and tracking error curves, respectively, for each joint of the robotic manipulator. These provide a clearer comparison between control strategies. Compared to the alternative control method, the proposed control approach clearly demonstrates better performance, as evidenced by its shorter convergence time and enhanced steady-state tracking accuracy. These simulation results clearly showcase the improved performance and efficiency of the proposed control technique compared to other control methods. Figure 12 shows the lumped disturbances and their estimation. The control inputs for the proposed FTTSMC and Boukattaya et al.'s[50] controller are shown in Figures 13 and 14, respectively. As demonstrated in Figure 13, the FTTSMC method effectively mitigates chattering. Boukattaya et al.'s[50] controller also generates a continuous control input, as depicted in Figure 14, by utilizing $\tanh\,(x/\varepsilon\,)\,, \varepsilon > 0$ instead of the function.[50] The comparison between the figures highlights that the proposed approach delivers better control performance with lower control input signals compared to the alternative controller.

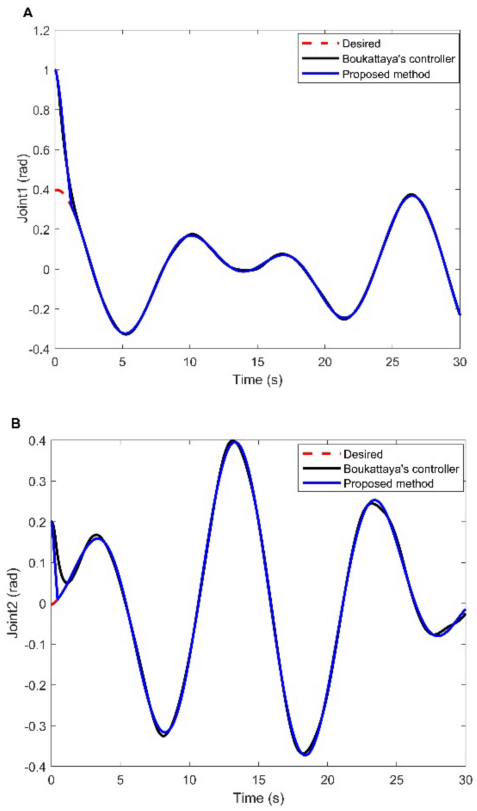

Figure 10. Position tracking for (A) joint 1 and (B) joint 2

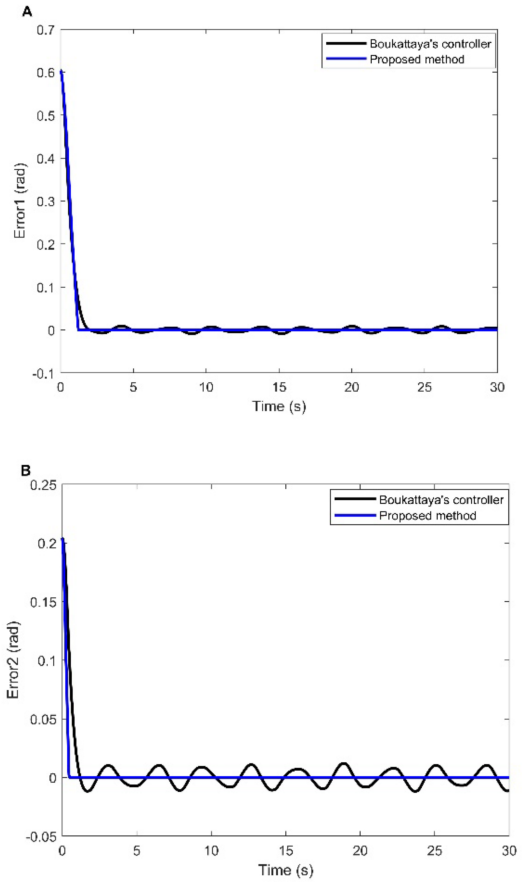

Figure 11. Position tracking errors for (A) joint 1 and (B) joint 2

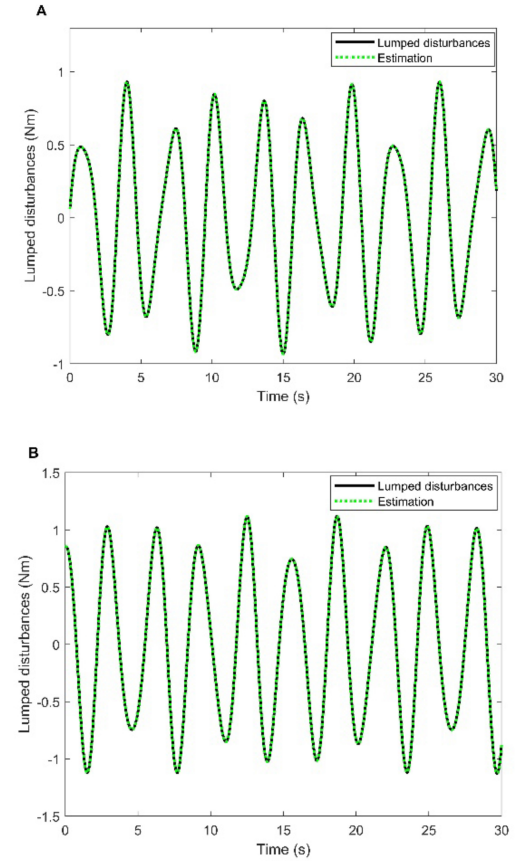

Figure 12. Estimation of lumped disturbances for (A) joint 1 and (B) joint 2

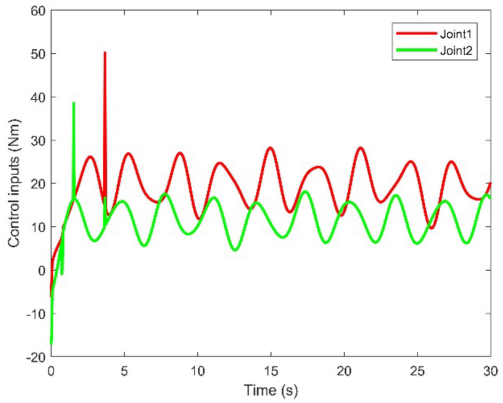

Figure 13. Control inputs for the proposed fixed-time trajectory tracking sliding mode control

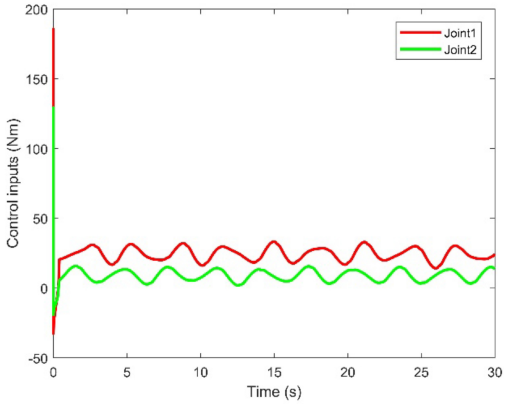

Figure 14. Control inputs for Boukattaya et al.'s controller

5. Conclusion

The study introduces a robust trajectory tracking control approach for uncertain nonlinear dynamic systems by leveraging a fixed-time DO. First, a novel FVECDO was designed using fixed-time stability theory to accurately estimate the combined uncertainties arising from modeling inaccuracies and external disturbances. Utilizing the information from this DO, a sliding mode control strategy was proposed that ensures fixed-time convergence for trajectory tracking. This approach incorporated a reaching law with a state-dependent exponent coefficient in conjunction with a sliding variable designed for fixed-time convergence. The developed controller exhibited key advantages, including high robustness, reduced chattering, and avoidance of singularities. Lyapunov theory was employed to comprehensively analyze the system's fixed-time stability and control precision. Finally, simulations comparing this method with other control strategies demonstrated its effectiveness and low sensitivity to the system's initial conditions. Future work will explore the controller's performance in

the presence of measurement noise and additional nonlinearities, such as dead zones and input saturation, along with experimental validation of the proposed approach. In addition, the proposed fixed-time control framework could be extended to fractional-order systems, which may further enhance control precision and robustness in complex nonlinear environments.

Acknowledgments

None.

Funding

The authors would like to thank the Natural Science Funding of Fujian Province, China (Grant/Award Number: 2024J011561) for their support in this research.

Conflict of interest

The authors declare that they have no conflict of interest regarding the publication of this article.

Author contributions

Conceptualization: Zeeshan Anjum, Wen-Jer Chang
Formal analysis: Zeeshan Anjum, Muhammad Shamrooz Aslam, Rizwan Ullah
Investigation: Zeeshan Anjum, Wen-Jer Chang, Muhammad Shamrooz Aslam
Methodology: Zeeshan Anjum, Rizwan Ullah
Writing–original draft: Zeeshan Anjum, Wen-Jer Chang
Writing–review & editing: Zeeshan Anjum, Wen-Jer Chang, Muhammad Shamrooz Aslam

Availability of data

Not applicable.

AI tools statement

All authors confirm that no AI tools were used in the preparation of this manuscript.

References

1. Nikdel N, Badamchizadeh M, Azimirad V, Nazari M. Adaptive backstepping control for an n-degree of freedom robotic manipulator based on combined state augmentation. *Rob Comput Integr Manuf.* 2017;44:129-143. https://doi.org/10.1016/j.rcim.2016.08.007
2. Aslam MS, Tiwari P, Pandey HM, Band SS, El Sayed H. A delayed Takagi–Sugeno fuzzy control approach with uncertain measurements using an extended sliding mode observer. *Inf Sci (NY).* 2023;643:119204. https://doi.org/10.1016/j.ins.2023.119204
3. Aslam MS, Zhenhua M, Ullah R, Li Y, Sheng A, Majid A. Stability and admissibility analysis of T–S descriptive systems and its applications. *Soft Comput.* 2022;26(15):7159-7166. https://doi.org/10.1007/s00500-022-07323-1
4. Purwar S, Kar IN, Jha AN. Adaptive output feedback tracking control of robot manipulators using position measurements only. *Expert Syst Appl.* 2008;34(4):2789-2798. https://doi.org/10.1016/j.eswa.2007.05.030
5. Shojaei K, Shahri AM, Tarakameh A. Adaptive feedback linearizing control of nonholonomic wheeled mobile robots in presence of parametric and nonparametric uncertainties. *Rob Comput Integr Manuf.* 2011;27(1):194-204. https://doi.org/10.1016/j.rcim.2010.07.007
6. Kaveh A, Vahedi M, Gandomkar M. Improving the performance of a chaotic nonlinear system of fractional-order brushless direct current electric motor using fractional-order sliding mode control. *Int J Optim Control: Theor Appl.* 2025;15(3): 379-395. https://doi.org/10.36922/ijocta.8407
7. Yavuz M, Öztürk M, Yaşkıran B. Comparison of fractional order sliding mode controllers on robot manipulator. *Int J Optim Control: Theor Appl.* 2025;15(2):281-293. https://doi.org/10.36922/ijocta.1678
8. Mohan Raja M, Vijayakumar V, Veluvolu KC, Shukla A, Nisar KS. Existence and optimal control results for Caputo fractional delay Clark's sub differential inclusions of order r (1,2) with sectorial operators. *Optim Control Appl Methods.* 2024;45(4):1832-1850. https://doi.org/10.1002/oca.3125
9. Raja MM, Vijayakumar V, Veluvolu KC. Improved order in Hilfer fractional differential systems: solvability and optimal control problem for hemivariational inequalities. *Chaos Solitons Fractals.* 2024;188:115558. https://doi.org/10.1016/j.chaos.2024.115558
10. Shtessel Y, Edwards C, Fridman L, Levant A. *Sliding Mode Control and Observation.* Vol 10. Springer; 2014.
11. Aslam MS, Qaisar I, Majid A, Ramaraj P. Design of sliding mode controller for sensor/actuator fault with unknown input observer for satellite control system. *Soft Comput.* 2021;25(24):14993-15003. https://doi.org/10.1007/s00500-021-06420-x
12. Ren C, Li X, Yang X, Ma S. Extended state observer-based sliding mode control of an omnidirectional mobile robot with friction compensation. *IEEE Trans Ind Electron.* 2019;66(12):9480-9489. https://doi.org/10.1109/TIE.2019.2892678
13. Venkataraman S, Gulati S. *Control of Nonlinear Systems Using Terminal Sliding Modes.* IEEE; 1993.
14. Zuo Z. Non-singular fixed-time terminal sliding mode control of non-linear systems. *IET Control*

Theory Appl. 2015;9(4):545-552. https://doi.org/10.1049/iet-cta.2014.0202
15. Ahmed S, Azar AT. Predefined-time fractional-order terminal SMC for robot dynamics. *Int J Optim Control: Theor Appl.* 2025;15(3):426-434. https://doi.org/10.36922/IJOCTA025060020
16. Feng Y, Yu X, Man Z. Non-singular terminal sliding mode control of rigid manipulators. *Automatica.* 2002;38(12):2159-2167. https://doi.org/10.1016/S0005-1098(02)00147-4
17. Yu S, Yu X, Shirinzadeh B, Man Z. Continuous finite-time control for robotic manipulators with terminal sliding mode. *Automatica.* 2005;41(11):1957-1964. https://doi.org/10.1016/j.automatica.2005.07.001
18. Wang L, Chai T, Zhai L. Neural-network-based terminal sliding-mode control of robotic manipulators including actuator dynamics. *IEEE Trans Ind Electron.* 2009;56(9):3296-3304. https://doi.org/10.1109/TIE.2008.2011350
19. Bakouri M, Alqarni A, Alanazi S, et al. Robust dynamic control algorithm for uncertain powered wheelchairs based on sliding neural network approach. *AIMS Math.* 2023;8(11):26821-26839. https://doi.org/10.3934/math.20231373
20. Ghasemi M, Nersesov SG. Finite-time coordination in multiagent systems using sliding mode control approach. *Automatica.* 2014;50(4):1209-1216. https://doi.org/10.1016/j.automatica.2014.02.019
21. Feng Y, Yu X, Han F. On nonsingular terminal sliding-mode control of nonlinear systems. *Automatica.* 2013;49(6):1715-1722. https://doi.org/10.1016/j.automatica.2013.01.051
22. Polyakov A. Nonlinear feedback design for fixed-time stabilization of linear control systems. *IEEE Trans Autom Control.* 2011;57(8):2106-2110. https://doi.org/10.1109/TAC.2011.2179869
23. Wang C, Tnunay H, Zuo Z, Lennox B, Ding Z. Fixed-time formation control of multirobot systems: design and experiments. *IEEE Trans Ind Electron.* 2018;66(8):6292-6301. https://doi.org/10.1109/TIE.2018.2870409
24. Du H, Wen G, Wu D, Cheng Y, Lü J. Distributed fixed-time consensus for nonlinear heterogeneous multi-agent systems. *Automatica.* 2020;113:108797. https://doi.org/10.1016/j.automatica.2019.108797
25. Pan Y, Du P, Xue H, Lam HK. Singularity-free fixed-time fuzzy control for robotic systems with user-defined performance. *IEEE Trans Fuzzy Syst.* 2020;29(8):2388-2398. https://doi.org/10.1109/TFUZZ.2020.2999746
26. Golestani M, Esmaeilzadeh SM, Mobayen S. Fixed-time control for high-precision attitude stabilization of flexible spacecraft. Eur J Control. 2021;57:222-231. https://doi.org/10.1016/j.ejcon.2020.05.006
27. Zhang L, Wei C, Jing L, Cui N. Fixed-time sliding mode attitude tracking control for a submarine-launched missile with multiple disturbances. *Nonlinear Dyn.* 2018;93:2543-2563. https://doi.org/10.1007/s11071-018-4341-8
28. Ni J, Liu L, Liu C, Hu X, Li S. Fast fixed-time nonsingular terminal sliding mode control and its application to chaos suppression in power system. *IEEE Trans Circuits Syst II Exp Briefs.* 2016;64(2):151-155. https://doi.org/10.1109/TCSII.2016.2551539
29. Wang L, Du H, Zhang W, Wu D, Zhu W. Implementation of integral fixed-time sliding mode controller for speed regulation of PMSM servo system. *Nonlinear Dyn.* 2020;102:185-196. https://doi.org/10.1007/s11071-020-05938-3
30. Zuo Z, Tie L. A new class of finite-time nonlinear consensus protocols for multi-agent systems. *Int J Control.* 2014;87(2):363-370. https://doi.org/10.1080/00207179.2013.834484
31. Chen C, Li L, Peng H, et al. A new fixed-time stability theorem and its application to the fixed-time synchronization of neural networks. *Neural Netw.* 2020;123:412-419. https://doi.org/10.1016/j.neunet.2019.12.028
32. Zhao L, Jia Y. Decentralized adaptive attitude synchronization control for spacecraft formation using nonsingular fast terminal sliding mode. *Nonlinear Dyn.* 2014;78:2779-2794. https://doi.org/10.1007/s11071-014-1625-5
33. Chen M, Wu QX, Cui RX. Terminal sliding mode tracking control for a class of SISO uncertain nonlinear systems. *ISA Trans.* 2013;52(2):198-206. https://doi.org/10.1016/j.isatra.2012.09.009
34. Yang J, Li S, Yu X. Sliding-mode control for systems with mismatched uncertainties via a disturbance observer. *IEEE Trans Ind Electron.* 2012;60(1):160-169. https://doi.org/10.1109/TIE.2012.2183841
35. Hua C, Li J, Yang Y, Guan X. Extended-state-observer-based finite-time synchronization control design of teleoperation with experimental validation. *Nonlinear Dyn.* 2016;85:317-331. https://doi.org/10.1007/s11071-016-2687-3
36. Li S, Sun H, Yang J, Yu X. Continuous finite-time output regulation for disturbed systems under mismatching condition. *IEEE Trans Autom Control.* 2014;60(1):277-282. https://doi.org/10.1109/TAC.2014.2324212
37. Chen WH, Yang J, Guo L, Li S. Disturbance-observer-based control and related methods—an overview. *IEEE Trans Ind Electron.* 2015;63(2):1083-1095. https://doi.org/10.1109/TIE.2015.2478397
38. Zhang L, Wei C, Wu R, Cui N. Fixed-time extended state observer based non-singular fast terminal sliding mode control for a VTVL reusable launch vehicle. *Aerosp Sci Technol.* 2018;82:70-79. https://doi.org/10.1016/j.ast.2018.08.028
39. Ding B, Xu D, Jiang B, Shi P, Yang W. Disturbance-observer-based terminal sliding

mode control for linear traction system with prescribed performance. *IEEE Trans Transp Electrific.* 2020;7(2):649-658. https://doi.org/10.1109/TTE.2020.3027367
40. Zhang CH, Yang GH. Event-triggered global finite-time control for a class of uncertain nonlinear systems. *IEEE Trans Autom Control.* 2019;65(3):1340-1347. https://doi.org/10.1109/TAC.2019.2928767
41. Liu S, Niu B, Zong G, Zhao X, Xu N. Adaptive fixed-time hierarchical sliding mode control for switched under-actuated systems with dead-zone constraints via event-triggered strategy. *Appl Math Comput.* 2022;435:127441. https://doi.org/10.1016/j.amc.2022.127441
42. Wu Y, Li G, Zuo Z, Liu X, Xu P. Practical fixed-time position tracking control of permanent magnet DC torque motor systems. *IEEE/ASME Trans Mechatron.* 2020;26(1):563-573. https://doi.org/10.1109/TMECH.2020.3042806
43. Cao S, Sun L, Jiang J, Zuo Z. Reinforcement learning-based fixed-time trajectory tracking control for uncertain robotic manipulators with input saturation. *IEEE Trans Neural Netw Learn Syst.* 2021;34(8):4584-4595. https://doi.org/10.1109/TNNLS.2021.3116713
44. Rezaei E, Bolandi H, Fathi M. Designing a fixed-time observer-based adaptive non-singular sliding mode controller for flexible spacecraft. *ISA Trans.* 2024;148:32-44. https://doi.org/10.1016/j.isatra.2024.03.025
45. Yang C, Teng T, Xu B, Li Z, Na J, Su CY. Global adaptive tracking control of robot manipulators using neural networks with finite-time learning convergence. *Int J Control Autom Syst.* 2017;15(4):1916-1924. https://doi.org/10.1007/s12555-016-0515-7
46. Li H, Cai Y. On SFTSM control with fixed-time convergence. *IET Control Theory Appl.* 2017;11(6):766-773. https://doi.org/10.1049/iet-cta.2016.1457
47. Yang L, Yang J. Nonsingular fast terminal sliding-mode control for nonlinear dynamical systems. *Int J Robust Nonlinear Control.* 2011;21(16):1865-1879. https://doi.org/10.1002/rnc.1666
48. Moulay E, Léchappé V, Bernuau E, Plestan F. Robust fixed-time stability: Application to sliding-mode control. *IEEE Trans Autom Control.* 2021;67(2):1061-1066. https://doi.org/10.1109/TAC.2021.3069667
49. Zhai J, Xu G. A novel non-singular terminal sliding mode trajectory tracking control for robotic manipulators. *IEEE Trans Circuits Syst II Exp Briefs.* 2020;68(1):391-395. https://doi.org/10.1109/TCSII.2020.2999937
50. Boukattaya M, Mezghani N, Damak T. Adaptive nonsingular fast terminal sliding-mode control for the tracking problem of uncertain dynamical systems. *ISA Trans.* 2018;77:1-19. https://doi.org/10.1016/j.isatra.2018.04.007

Zeeshan Anjum *received his Ph.D. in Control Science and Engineering from Nanjing University of Science and Technology, China. He completed his postdoctoral research at Zhejiang University of Technology, focusing on robust control of uncertain nonlinear systems. He is currently serving as an Associate Professor at Quanzhou University of Information Engineering. His research interests include fixed-time and finite-time control, sliding mode control, fault-tolerant control, and adaptive control of robotic manipulators and nonlinear systems. Dr. Anjum has published several papers in prestigious international journals and actively contributes as a reviewer for leading journals.*
https://orcid.org/0000-0002-8016-4165

Wen-Jer Chang *received the Ph.D. degree from the Institute of Electrical Engineering of the National Central University in 1995. Since 1995, he has been with the National Taiwan Ocean University (NTOU), Keelung, Taiwan. He is currently a Distinguished Professor of the Department of Marine Engineering and the Director of the Center for Social Responsibility and Sustainable Development of NTOU. Since 2021, he has been the Chairman of the Association of Marine Affairs. In 2022, he was elected to the grade of IEEE Senior Member. From 2021 to 2024, he is listed in the "World's Top 2% Scientists," according to Stanford University. Dr. Chang has authored more than 300 published journal papers and conference papers. His recent research interests are intelligent control, fuzzy control, robust control, marine engineering, and smart shipping.*
https://orcid.org/0000-0001-5054-8451

Muhammad Shamrooz Aslam *received his B.Sc. and M.S. degrees in Electronics and Electrical Engineering from COMSATS University, Pakistan, in 2009 and 2013, respectively, and his Ph.D. in Control Science and Engineering from Nanjing University of Science and Technology, China, in 2019. He has served as a Lecturer at COMSATS University, a Visiting Lecturer at Edinburgh Napier University (UK) and Southern Cross University (Australia), and an Associate Professor at Guangxi University of Science and Technology, China. He is currently an Assistant Professor at the Artificial Intelligence Research Institute, China University of Mining and Technology. His research focuses on fuzzy systems, time-delay systems, nonlinear systems, and network control systems. Dr. Aslam is an active*

reviewer for top journals, including IEEE Transactions, Nonlinear Dynamics, and Fuzzy Sets and Systems.

https://orcid.org/0000-0002-7622-1788

Rizwan Ullah *received his B.S. in Electronics Engineering from COMSATS University, Abbottabad campus, Pakistan, in 2009, and his M.S. in Electrical Engineering from COMSATS University, Attock campus, Pakistan, in 2013. He served as a Lecturer at COMSATS University, Attock campus, from 2013 to 2017. He holds a Ph.D. degree from the School of Automation, Nanjing University of Science and Technology, China. Currently, he is an Associate Professor at the School of Mechanical and Electrical Engineering, Quanzhou University of Information Engineering. His research interests include network control systems, fuzzy systems, time-delay systems, nonlinear systems, multi-agent systems, and reinforcement learning.*

https://orcid.org/0000-0001-9218-5281

An International Journal of Optimization and Control: Theories & Applications
(https://accscience.com/journal/ijocta)

This work is licensed under a Creative Commons Attribution 4.0 International License. The authors retain ownership of the copyright for their article, but they allow anyone to download, reuse, reprint, modify, distribute, and/or copy articles in IJOCTA, so long as the original authors and source are credited. To see the complete license contents, please visit http://creativecommons.org/licenses/by/4.0/.